

ONB, OSV, and OFI for subcooled flow boiling through a narrow rectangular channel heated on one-side



Omar S. Al-Yahia, Daeseong Jo*

School of Mechanical Engineering, Kyungpook National University, 80 Daehak-ro, Buk-gu, Daegu 702-701, Republic of Korea

ARTICLE INFO

Article history:

Received 22 April 2017

Received in revised form 1 September 2017

Accepted 5 September 2017

Available online 14 September 2017

Keywords:

Subcooled boiling

Upward flow

Rectangular channel

ONB

OSV

OFI

ABSTRACT

This paper presents an experimental investigation of the thermal hydraulic thresholds of the subcooled boiling instability in forced convective flow, such as the onset of nucleate boiling (ONB), the onset of significant void (OSV), and the onset of flow instability (OFI). The experiment was constrained to water flows in the upward direction under atmospheric pressure through a narrow rectangular channel heated on one-side having a gap of 2.35 mm, a width of 54 mm, and length of 566 mm. The heated length and width were 300 mm and 50 mm, respectively. The experiment was performed over a wide range of inlet temperature (35–65 °C), mass fluxes (118–1400 kg/(m²s)), and heat fluxes (50–650 kW/m²). Two experimental methods were adopted to achieve and identify the ONB, OSV, and OFI: (1) the constant mass flow rate approach and (2) the constant heat flux approach. The results showed consistency between the two methods. The ONB was identified through visualized monitoring using a high-speed camera and by using the slope of the wall temperature deviation method. The ONB was predicted by Jens and Lottes' correlation. The OSV was detected using the high-speed camera and the wall temperature–heat flux curve. Based on the experimental method, the OFI was identified using pressure drop and inlet pressure fluctuation. The data showed that the OSV and OFI could occur at similar points based on the experimental conditions. Furthermore, the OSV models, such as the modified Bowring model and Saha and Zuber's model, can be used to predict the OFI. Additionally, some OFI correlations showed good agreement with the present data. However, many other correlations underestimated the OFI results, which might have been a result of differences in the experimental parameters. Therefore, a new empirical correlation that predicted the present data and other experimental data within very good accuracy was suggested. The present study describes and discusses the influence of the experimental parameters; inlet subcooling, mass flow rate, and the imposed heat flux on the ONB, OSV, and OFI incipience.

© 2017 Elsevier Ltd. All rights reserved.

1. Introduction

In the past decades, the use of subcooled flow boiling in narrow rectangular channels in compact volume systems has significantly grown, owing to its high heat transfer capabilities. Supercomputer systems, nuclear research reactors, heat exchangers, fusion energy, and many other applications are examples of compact volumes [1,2]. The subcooled flow boiling region lies between two distinct thermal hydraulic behaviors; onset of nucleate boiling (ONB) and onset of flow instability (OFI). Understanding and identifying these behaviors is very important for reliable and safe operation of any two-phase flow system. In subcooled flow boiling, the coolant enters the channel as a single-phase liquid with a highly subcooled temperature. As illustrated in Fig. 1, as the coolant flows through

the channel, the bulk and wall temperatures increase. Once the wall temperature exceeds the saturation temperature of the coolant [3], nucleation occurs within small activated cavities on the heated surface. This phenomenon is known as the ONB, and it is the threshold point between single-phase and two-phase flow. The ONB is identified using wall temperature measurements and pressure drop monitoring; it is the point where the slope of the pressure drop–mass flow rate curve deviates from the single-phase line. In addition, the ONB is identified as the intersection point between single-phase and two-phase heat transfer on the wall temperature–heat flux curve. ONB is local phenomenon on the heated surface, which depends on the local thermal hydraulic parameters, regardless to geometry shapes of flows. After ONB, the generated bubbles condense directly when they are detached from the wall owing to the high degree of subcooling in the liquid core. However, if the departing bubbles survive condensation, the void fraction starts growing significantly [4], and a fully developed

* Corresponding author.

E-mail address: djo@knu.ac.kr (D. Jo).

Nomenclature

A_h	heated area [m^2]
A_s	cross sectional area [m^2]
C_p	heat capacity [$\text{J}/(\text{kg K})$]
D_h	hydraulic diameter [m]
G	mass flux [$\text{kg}/(\text{m}^2 \text{s})$]
h	convective heat transfer coefficient [$\text{W}/(\text{m}^2 \text{K})$]
L_h	heated length [m]
\dot{m}	mass flow rate [kg/s]
Nu	Nusselt number
P_h	heated perimeter
P_w	wetted perimeter
P	pressure [bar]
Pe	Peclet number = $PrRe$
Pr	Prandtl Number = $\frac{\mu C_p}{k}$
Q	power [W]
Re	Reynolds number = $\frac{\rho v D_h}{\mu}$
T	temperature [$^\circ\text{C}$]
k	thermal conductivity [$\text{W}/(\text{m K})$]
q''	heat flux [W/m^2]
t	thickness [m]

Greek symbols	
μ	viscosity [$\text{kg}/(\text{s m})$]
ρ	density [kg/m^3]

Subscripts	
ONB	onset of nucleate boiling
OSV	onset of significant void
OFI	onset of flow instability
<i>b</i>	bulk
<i>e</i>	electrical
<i>i</i>	inlet
<i>l</i>	liquid
<i>o</i>	outlet
<i>sat</i>	saturation
<i>sub</i>	subcooled
<i>th</i>	thermal
TC	thermocouple
<i>w</i>	wall

nucleate boiling regime dominates. This phenomenon is known as the onset of significant void (OSV) or net vapor generation (NVG). Beyond the OSV, the heat transfer coefficient achieved its highest value, whereas the heated surface temperature remains constant and/or slightly reduced in some cases. The void fraction distribution affects the flow instability, heat transfer rate, and pressure drop of the flow systems. Therefore, with further increase in the void fraction, the mass and heat transfer conditions become unstable [5]. This phenomenon is called the onset of flow instability (OFI). The OFI is the restricted threshold point for two-phase flow for reliable and safe operation, especially if flow occurs in a narrow rectangular channel, to avoid any undesirable events, such as critical heat flux (CHF). Additionally, the OFI is defined as the minimum point on the pressure drop-mass flow rate curve [6], as illustrated on Fig. 2. The OFI is controlled by three components of

pressure drop: the potential pressure drop, which stabilizes the system; the momentum pressure drop; and the friction pressure drop, which destabilize the system [7].

Several experimental and numerical studies have been performed to investigate the ONB behavior in conventional and narrow channels [8–12]. Based on the findings of these studies, various correlations have been proposed to estimate the ONB, such as the Bergles and Rohsenow [9], Jens and Lottes [10], and Thom et al. [11] correlations, as listed in Eqs. (1), (2) and (3), respectively.

$$\Delta T_{ONB} = \frac{5}{9} \left[\frac{q''_{ONB}}{1082P^{1.156}} \right]^{\frac{0.0234}{2.16}} \quad (1)$$

$$\Delta T_{ONB} = 25 \left[\frac{q''_{ONB}}{10^6} \right]^{0.25} \exp\left(-\frac{P}{6.2}\right) \quad (2)$$

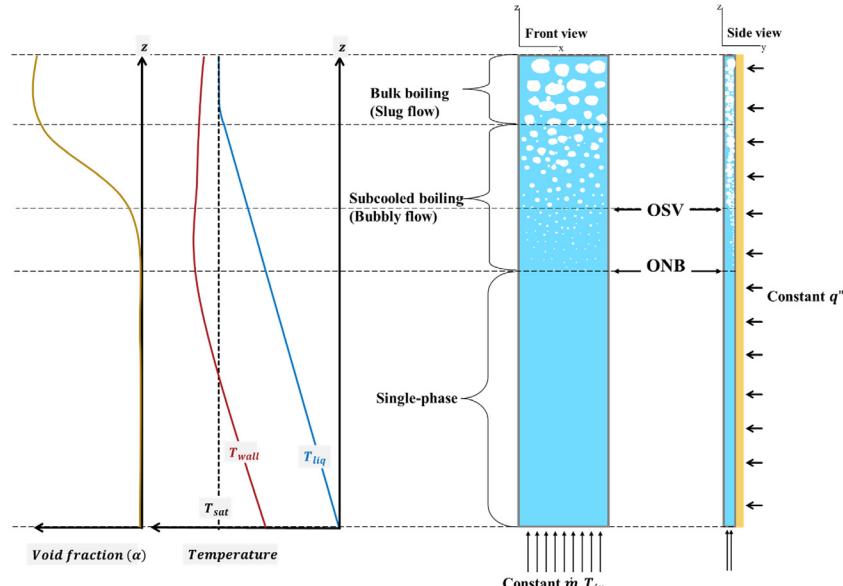


Fig. 1. Transition process from single-phase to two-phase flow.

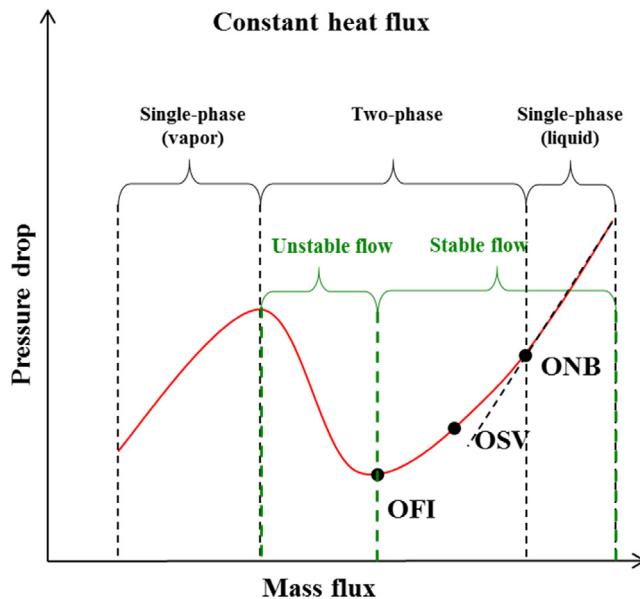


Fig. 2. Pressure drop-mass flux curve at a given heat flux and inlet degree of subcooling.

$$\Delta T_{ONB} = 22.65 \left[\frac{q''_{ONB}}{10^6} \right]^{0.5} \exp\left(-\frac{P}{8.7}\right) \quad (3)$$

Sudo et al. [12] performed ONB experiment for downward and upward flow through a narrow rectangular channel. There were no significant differences between upward and downward flow on the ONB incipience. Although Bergles and Rohsenow's [9] correlation was developed based on round tube, it predicted their results well within an error of 1 K. Experimentally, the incipience of ONB is observed using several methods: (1) pressure drop measurement [13,14]; (2) axial wall temperature measurement [15,16], where the slope of the axial temperature distribution decreases once the ONB occurs; (3) wall temperature measurement while the heat flux increases, in which the slope of the wall temperature-heat flux curve decreases at the ONB [17,18]; and (4) direct visualization using a high speed camera [19,20]. In 2014, Wang et al. [21] used four different methods to identify the ONB through a narrow rectangular channel: (1) the variation of the pressure drop with the mass flux, (2) the variation of the pressure drop with the heat flux, (3) the variation of the heat transfer coefficient with the mass flux, and (4) the variation of the heat transfer coefficient with the heat flux; however, they did not find significant differences between them. The authors got good agreement between their experimental results and Thom et al. correlation [11]. Recently, Yang et al. [22] experimentally studied the incipience of ONB for subcooled forced convection boiling through a narrow rectangular channel. They used the wall temperature versus heat flux curve to identify the ONB, and compared their findings with the visual inspection of the bubbles on the heated surface. Based on their experimental results, they developed new model to predict the ONB, such as

$$\Delta T_{ONB} = \left[\frac{q''_{ONB}}{2454} \right]^{0.5} \quad (4)$$

The OSV is not sharply defined, falling instead within a range. Furthermore, it is not characterized by the detachment of the first bubble from the wall or ejection from a wall bubbly layer [23]. However, it can be identified as the location that experiences a sudden increase in its void fraction. The OSV has been examined experimentally and theoretically, mostly in uniformly heated conventional channels. Experimentally, there are several methods that can be used to observe the void fraction, with the most common

and simplest one being direct visualization using a high speed camera [24,25]. Other methods are used to measure the axial distribution on the area-averaged void fraction based on the radiation reflection, such as gamma-ray densitometry and X-radiography [26–28]. The local void can be also measured by thermal and electrical probes; however, they cannot be used in narrow channels. Fiber-optics lasers are one of the newest methods that are used to measure the local void fraction [29]. After detecting the void fraction, the OSV is determined as the maximum increasing rate point of the void fraction curve. Several empirical correlations and theoretical models that predict the OSV exist. There are three categories of OSV models [23]. The first is the thermal hydrodynamically model, which is based on correlating the heat transfer rate at the OSV. In the second category, the OSV is considered to be the point at which the first bubble departs from the heated surface. In the third category, OSV is the point where the bubbles leave the wall bubbly layer and enter the subcooled bulk. In 1962, Bowring [30] proposed an empirical correlation to predict the OSV for water flows within a pressure range of 1.1–13.8 MPa, as follow:

$$\Delta T_{sub(OSV)} = (14 + P) \times 10^{-6} \frac{\rho_l q}{G} \quad (5)$$

As expressed in Bowring's correlation, the subcooling degree at the OSV reduces once the mass flux through the channel increases. The Saha and Zuber [31] correlation is one of the most common and accurately predictive model that can be used to estimate the OSV [32]. They argued that the OSV depends on only the local thermal conditions for low mass flow rates and on local fluid dynamic conditions for high mass flow rates, regardless to the flow direction. Furthermore, they stated that the void fraction has two distinct behaviors depending on the Peclet number (Pe), which are

$$\begin{aligned} \Delta T_{sub(OSV)} &= 0.0022 \frac{q'' D_h}{k} \quad Pe < 70,000 \\ \Delta T_{sub(OSV)} &= 154 \frac{q''}{GC_{pl}} \quad Pe > 70,000 \end{aligned} \quad (6)$$

In 1975, Unal [33] argued that bubble detachment does not represent the incipience of OSV. Using the thermal-hydro dynamically based model and the assumption that the OSV is the transition point between subcooled boiling and fully developed boiling, they proposed an empirical relationship for subcooled boiling at the OSV that is valid when water is used as the working fluid with a high pressure range (0.1–15.8 MPa), mass flux (132–2818 kg/m²/s), and heat flux (150–1920 kW/m²), the correlation has no restriction on the flow direction:

$$\begin{aligned} \Delta T_{sub(OSV)} &= 0.24 \frac{q''}{h} \quad V \geq 0.45 \text{ m/s} \\ \Delta T_{sub(OSV)} &= 0.11 \frac{q''}{h} \quad V < 0.45 \text{ m/s} \end{aligned} \quad (7)$$

Edelman and Elias [34] studied the void fraction distribution inside a tube based on gamma attenuation and X-ray radiography. Their results were comparable to the correlation of Saha and Zuber [31] within an error of $\pm 25\%$. However, the existing correlations underestimate the OSV in a channel with a short heated length [35]. In 2011, Wang et al. [36] studied the ONB, OSV, and OFI on the demand curve in a one-side heated narrow rectangular channel. They modified Bowring [30] and Shah and Zuber [31] correlation by multiplying the RHS of Eqs. (5) and (6) by $\left(\frac{P_w}{P_h}\right)$ to reasonably predict the OSV in the one-side heated condition. The modified correlations are listed in Eqs. (8) and (9), respectively.

$$\Delta T_{sub(OSV)} = (14 + P) \times 10^{-6} \frac{\rho_l q''}{G} \left(\frac{P_w}{P_h} \right) \quad (8)$$

$$\begin{aligned} \Delta T_{sub(OSV)} &= 0.0022 \frac{q'' D_h}{k} \left(\frac{P_w}{P_h} \right) \quad Pe < 70,000 \\ \Delta T_{sub(OSV)} &= 154 \frac{q''}{GC_{pl}} \left(\frac{P_w}{P_h} \right) \quad Pe > 70,000 \end{aligned} \quad (9)$$

The two-phase flow instability is divided into static stability and dynamic instability [5]. For the static stability case, the threshold of unstable behavior can be predicted from the steady-state conservation laws. However, for dynamic instability, it is necessary to consider the dynamic effects, such as inertia, propagation time, and compressibility. The OFI generally occurs at slightly lower mass fluxes than the OSV on a pressure drop-mass flux curve, and it occurs at a slightly higher heat flux than the OSV on a pressure drop-heat flux curve. The OFI can be achieved by keeping the heat flux constant and decreasing the mass flux, or keeping the mass flux constant and increasing the heat flux [37].

Several empirical correlations have been suggested to estimate the minimum point on the pressure drop-mass flux curve that corresponds to the OFI. It is also known that the OSV correlations can be used to estimate the conservative values of the OFI [4]. Whittle and Forgan [6] conducted OFI experiments with five different test sections; four were narrow rectangular channels, and one was a round tube channel. They developed a formula to correlate the minima of the pressure drop-mass flux curve, which involves the ratio of the bulk temperature rise between the inlet and the outlet to the inlet subcooling temperature (R), as follows:

$$R = \frac{T_{out} - T_{in}}{T_{sat} - T_{in}} = \frac{1}{1 + 25D_h L_h} \quad (10)$$

Kennedy et al. [37] used a mini tube to investigate the OFI, and proposed a simple correlation to predict the OFI for high mass flux (800–4500 kg/m²s), outlet pressure (3.44–10.34 bar), and heat flux (0–4000 kW/m²):

$$q''_{OFI} = 0.9 q''_{sat} \quad (11)$$

where q''_{sat} is the heat flux required to achieve the saturation conditions at the channel outlet. It can be simply calculated using the energy balance equation, as follows:

$$q''_{sat} = \frac{GA_s Cp(T_{sat} - T_{in})}{P_h L_h} \quad (12)$$

Similarity for the mass flux at OFI, G_{OFI} , can be evaluated using the mass flux corresponding to the saturated bulk temperature at the channel exit [37]:

$$G_{OFI} = 1.11 G_{sat} \quad (13)$$

where G_{sat} can be determined as

$$G_{sat} = \frac{q P_h L_h}{A_s Cp(T_{sat} - T_{in})} \quad (14)$$

Table 1
Experimental conditions used in the previous experimental studies.

	Geometry	(a × b × c) [*] [mm]	Flow direction	Pressure [barb]	Inlet subcooling [°C]	Mass flux [kg/m ² /s]	Heat flux [kW/m ²]
ONB	Present study	Narrow rectangular	50(54) × 2.35 × 300	Upward	1–1.3	36–66	118–1400
	Sudo et al. (1986)	Narrow rectangular	50(50) × 2.25 × 750	Upward and downward	1–1.2	28–85	70–150
	Wang et al. (2014)	Narrow rectangular	40(40) × 2.00 × 1100	Upward	2.0–20.0	26–80	100–1500
	Song et al. (2015)	Narrow rectangular	30(40) × 2.35 × 350	Downward	~1	56–76	800–1200
	Yang et al. (2016)	Narrow rectangular	20(28) × 2 × 199	Upward	~1	4.7–33.3	122–657
OFI	Whittle and Forgan (1967)	Narrow rectangular	25.4 × 3.225 × 609.6 25.4 × 2.44 × 406.4 25.4 × 2.03 × 406.4 25.4 × 1.4 × 533.4	Downward	1.17–1.86	25.2–65	600–9000
	Kennedy et al. (2000)	Tube	1.17 _D × 160 1.45 _D × 160	Horizontal	3.44–10.3	25–70	800–4500
	Wang et al. (2011)	Narrow rectangular	40(40) × 3 × 470	Upward	7.0–10	20.2–60.8	151–603
	Lee et al. (2013)	Narrow rectangular	30(40) × 2.5 × 350 30(40) × 3.3 × 350 30(40) × 4.1 × 350	Downward	~1	43–75	100–1000

* a is heated width, the value inside the parentheses is the channel width, and b is thickness; c is the heated length

Lee et al. [1] performed OFI experiments for downward flow in a narrow rectangular channel heated from both sides at nearly atmospheric pressure. They compared their experimental results with the predictions of different correlations, and proposed a new correlation shown in Eq. (15). The correlation is a function of the Nusselt number Nu and reflects the effect of the channel width (gap size); they achieved a better accuracy during OFI evaluation when the proposed correlation was utilized.

$$\frac{G_{OFI}}{G_{sat}} = 1.48 + \frac{10.6}{Nu^{0.65}} \quad (15)$$

Recently, Ghione et al. [2] assessed the prediction criteria for the flow instability in vertical narrow rectangular channels using an experimental database containing data from studies conducted by other researchers. The authors used the existing evaluation criteria of the ONB, OSV, and onset of fully developed boiling (FDB) to identify the OFI. A large margin of the OFI can be achieved using the ONB-based criteria. The OFI can be estimated conservatively by using the NVG-based criteria. They used the net vapor generation ratio (NVGR) to estimate the OFI based on the NVG criteria for Peclet number larger than 70,000, as follows:

$$NVGR = \frac{i_{l,sat} - i_l}{\Delta i_{sub,NVG}} \quad (16)$$

where $\Delta i_{sub,NVG}$ can be evaluated from NVG correlations, such as the one proposed by Saha and Zuber [31]. Once the ratio (Eq. (16)) is equal to 1 or smaller, the OFI occurs in the channel. Table 1 provides a summary of the operational conditions that were used for some of the other experimental studies.

Although the previous studies were performed to investigate the thermal hydraulic thresholds of subcooled boiling, ONB, OSV, and OFI, most of them studied these thresholds separately because they achieved the ONB and the OSV using different experimental procedures. In practice, those thermal hydraulic behaviors can occur concurrently in any two-phase flow system, depending on whether the operation conditions are normal or abnormal; besides, they may occur at constant heat flux or constant mass flux. On the other hand, few studies have investigated the influence of the operation conditions on the safety margin range. Hence, the present experimental study was performed to sequentially investigate the ONB, OSV, and OFI under constant heat flux and constant mass flux conditions. The present study provides further understanding for those points within a narrow rectangular channel heated from one-side and a better identification of the OSV phenomenon at dif-

ferent mass flow rates and subcooled temperatures. Additionally, it clarifies the relationship between the OSV and OFI. The influence of thermal hydraulic parameters on the prediction of ONB and OFI is discussed in detail. Visualization of the ONB, OSV, and OFI is performed using a high speed camera. A comparison is performed between the present data and the related proposed correlations. Some of the existing OSV and OFI models are modified so that they are applicable to the narrow rectangular channel heated from one-side, and a new empirical formula is proposed to accurately predict the OFI.

2. Experimental description

An experiment on upward subcooled flow boiling in a narrow rectangular channel was performed using deionized water under atmospheric pressure for a wide range of inlet boundary and flow conditions, as summarized in Table 2.

2.1. Experimental facility

The flow boiling experimental facility is schematically shown in Fig. 3. The experimental loop consists of a test section, water reservoir, condensing tank, plate-frame heat exchanger, centrifugal pump, coriolis mass flowmeter, cylindrical preheater, data acquisition system (DAQ), and supply pump. The arrangement of the components of the experimental facility is shown in Fig. 4, which displays the picture of the facility. The experimental loop is filled

with deionized water through the drain line using an external supply pump. The water is driven using the centrifugal pump (Grundfos CR5-5) with a steady mass flow rate measured by the coriolis mass flowmeter (RHEONIK RHM 12 GNT). The water flows through a 200 W preheater, which adjusts and controls the inlet temperature of the test section. Then, the water flows into the test section in an upward direction absorbing the heat that is generated from the heated surface (0–15 kW). The heated coolant exits the outlet of the test section and enters the water reservoir that is connected to the condensing tank, as illustrated in Fig. 3. The water then passes through a plate-frame type heat exchanger that removes the extra heat from the system. Two pressure transmitters and two thermocouples (K-type) are installed at the inlet and the outlet of the test section to measure the flow conditions. The pressure drop across the test section is measured by a pressure transmitter (ROSEMOUNT 3051S). Two control panels are used to control the power and pump speed (mass flow rate) separately. The experimental data are monitored using a compact system (NI-cDAQ-9174) with a personal computer. The NI-compact system has two signal input modules: a current input module (NI-9207) used to read the current signals that are delivered from the applied power, flowmeter, pressure transducers, and pressure transmitter; and a thermocouple input module (NI-9213) that is used to read the thermocouples (TCs)' signals in degrees Celsius.

2.2. Test section

The test section used in the present experiment is shown in Fig. 5. The rectangular flow channel with dimensions 2.35 mm (thickness) × 54 mm (width) was uniformly heated from one-side over a 300 mm (heated length) × 50 mm (heated width), and the other side of the channel was a polycarbonate transparent window that enabled direct observation of the bubble behavior on the heated surface. The coolant entered the channel at a distance 133 mm below the heated section, and exited the channel at a distance of 133 mm above the heated section; therefore, the overall length of the coolant channel was 566 mm. Table 3 summarizes the geometrical parameters of the test section.

Table 2
Experimental conditions.

Parameter	Value
Flow rate [kg/s]	0.015–0.170
Heat flux [kW/m ²]	60–650
Inlet temperature [°C]	35–65
Pressure	1–1.4 atm

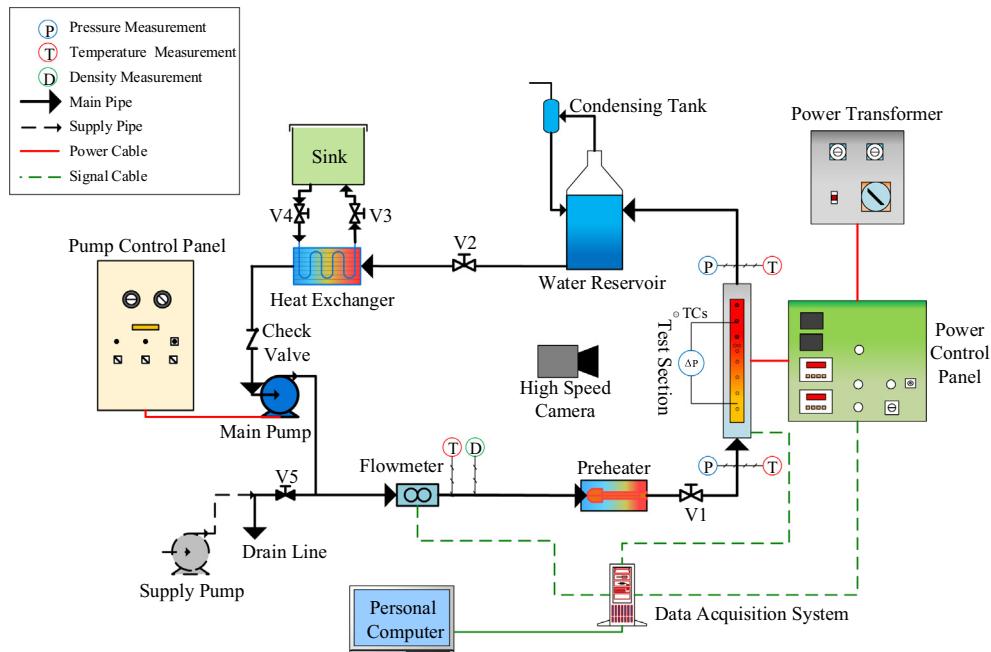


Fig. 3. Flow boiling experimental facility.

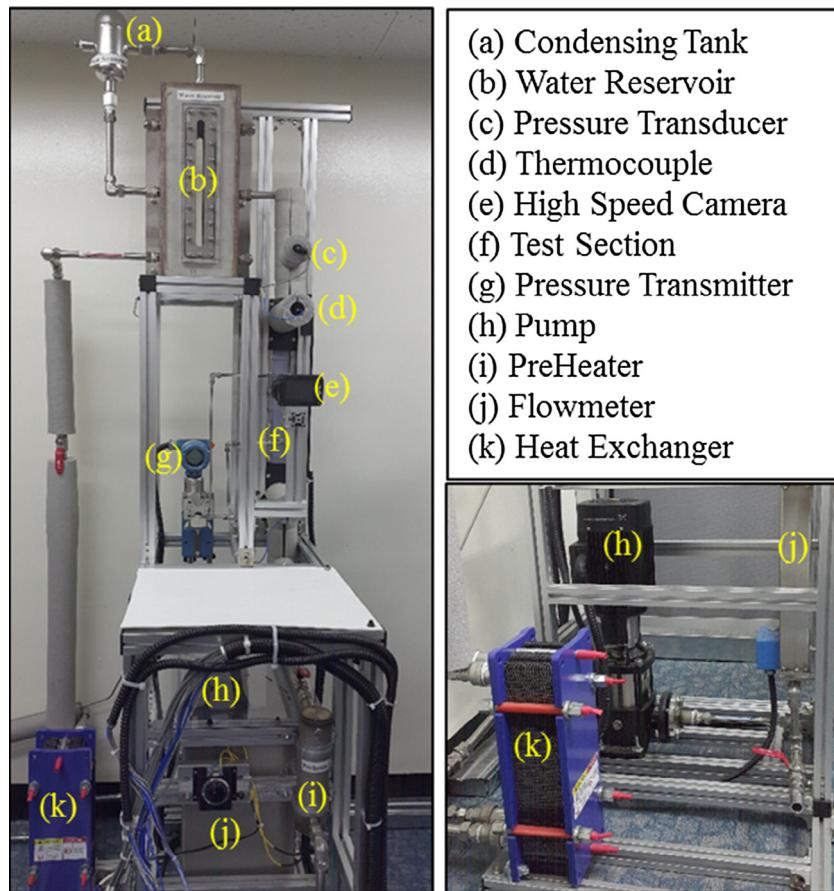


Fig. 4. A photograph of the experimental facility.

The heater body was an aluminum block with a thickness of 35 mm that used two stainless steel cartridge heaters (SUS316L) that were installed near the rear edge. The distance between the nearest point of the cartridge heaters and the channel surface (heated surface) was 17 mm, which was sufficient for the heated surface to reach a uniformity in heat flux. The SUS316L cartridge heaters were connected to a DC power supply system, where the applied power was controlled using a Thyristor Power Regulator (TPR). Ten K-type thermocouples (TCs) were inserted into the aluminum block to measure the temperature at 1.2 mm behind the heated surface; eight were distributed axially along the center line, and two were distributed transversely at 166 mm from the beginning of the heated surface, as illustrated in Fig. 5(a) and (c). Thereby, the temperature distribution in the transverse direction was observed. The pressure drop (ΔP) across the test section was measured using a pressure transmitter that was located as illustrated in Fig. 5(c).

2.3. Visualization technique

The bubble behavior and the void fraction through the narrow rectangular channel were analyzed using a high speed video. The front view of subcooled boiling at the heated surface was visualized directly using a high speed camera (Phantom Miro-EX4) with a high resolution of 512×512 at a recording rate of 2200 fps. The camera was focused on the centerline region of $20 \text{ mm} \times 20 \text{ mm}$, at distance of 166 mm from the beginning of the heated surface (Fig. 5(a)). The focal point of the camera was located on a series of TCs, which enabled the consistency between the thermocouple

measurement and the visual observation of the bubble formation to be checked.

2.4. Data reduction

Power was transmitted to the cartridge heaters in form of the electrical power, which is determined from the product of the applied voltage (V) and current (I) through the heaters, as

$$Q = VI \quad (17)$$

The cartridge heaters converted the electrical power to thermal power, which was transferred to the channel through the aluminum block. However, not all the electric power was transferred to the channel as thermal power, owing to heat losses to the surrounding environment. Therefore, the heat deposited into the channel could be determined from the sensible heat that was gained by the coolant under single-phase heat transfer conditions, as

$$Q_{th} = \dot{m}C_p(T_o - T_i) \quad (18)$$

where \dot{m} is the mass flow rate, C_p is the coolant specific heat, T_i is the coolant inlet temperature, and T_o is the coolant outlet temperature. The difference between the applied electrical power and the utilized thermal power is shown in Fig. 6; approximately 82–96% of the input electrical power was transferred as heat into the flow channel, as illustrated in Fig. 7, depending on the total power and mass flow rate.

The TCs were located in the aluminum block, and the distance between the tips of the TCs and the heating surface was 1.2 mm.

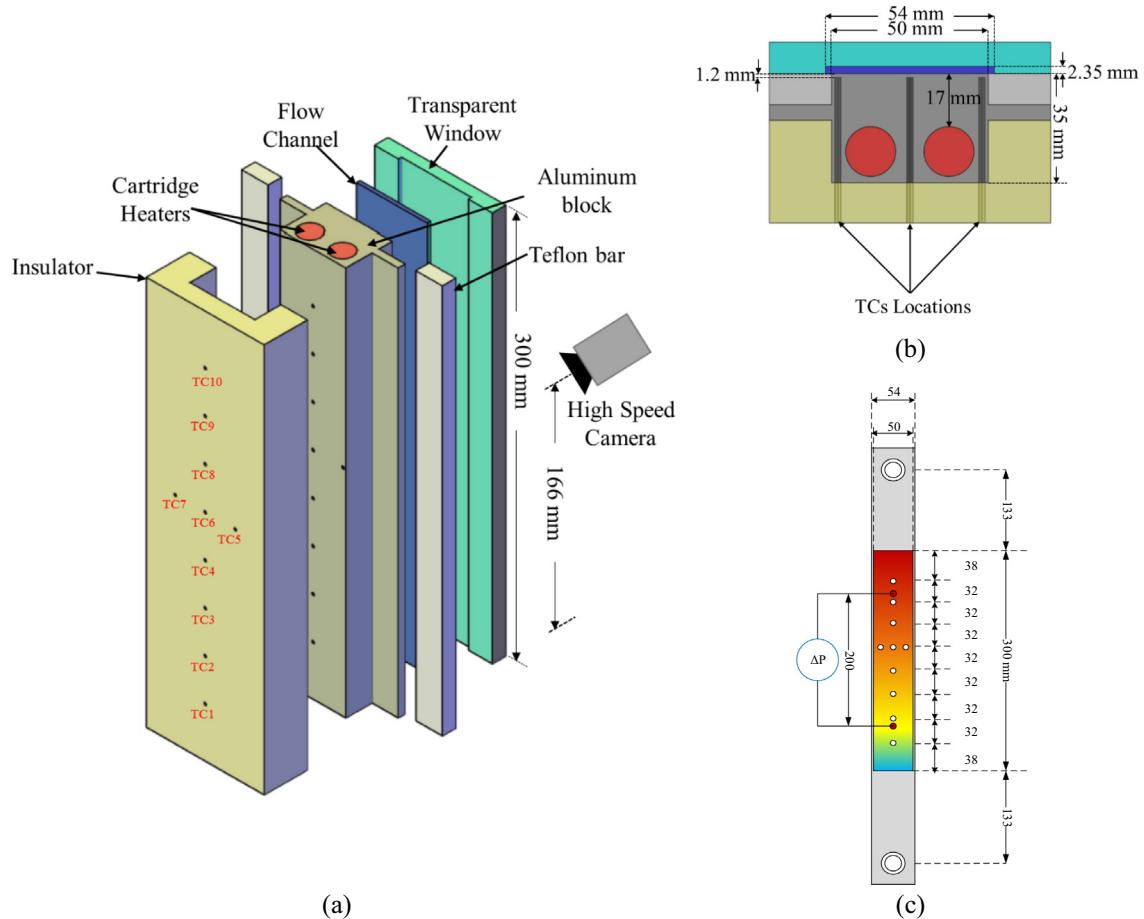


Fig. 5. Experimental test section: (a) 3D view of the heated section, (b) top view of the test section, and (c) front view of the test section.

Table 3
Geometrical parameters of the test section.

Parameter	Value
Channel thickness [mm]	2.35
Channel width [mm]	54
Channel length [mm]	566
Heated width [mm]	50
Heated length [mm]	300
Heated condition	One-side
Flow direction	Upward

The one-dimensional conduction equation was used to estimate the surface temperature based on the measured temperature, as follows:

$$T_w = T_{TC} - \left(\frac{Q_{th}}{A_h} \right) \frac{t}{k} \quad (19)$$

where T_w is the wall temperature on the flow side, T_{TC} is the measured temperature from the TCs, $\left(\frac{Q_{th}}{A_h} \right)$ is the average heat flux, t is the distance between the TCs and the wall (1.2 mm), and k is the thermal conductivity of the aluminum block. The bulk temperature is considered to linearly increase from the inlet to the outlet; as a result, the local bulk temperature is estimated as

$$T_b(z) = T_i + (T_o - T_i) \frac{z}{L_h} \quad (20)$$

where "z" is the distance from the entrance of the heater, and L_h is the total length of the heater.

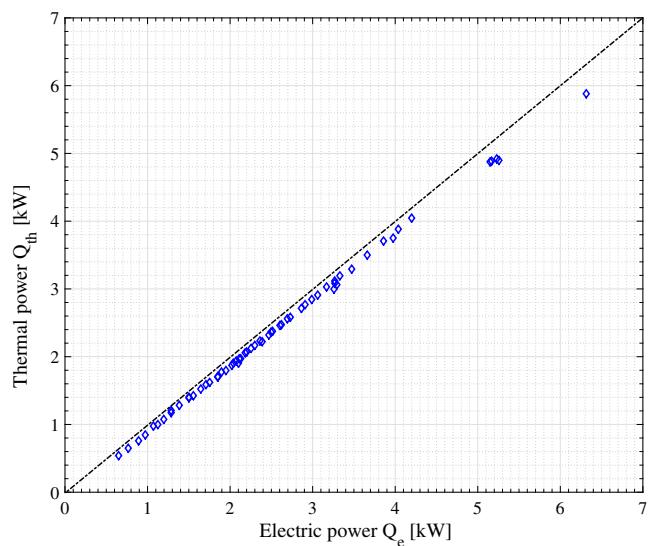


Fig. 6. Electric power versus thermal power.

2.5. Uncertainty analysis

The uncertainties associated with the experimental parameters were investigated in the present study. The parameters were categorized into geometry parameters (channel width and thickness, heated length and width), measured parameters (inlet and outlet

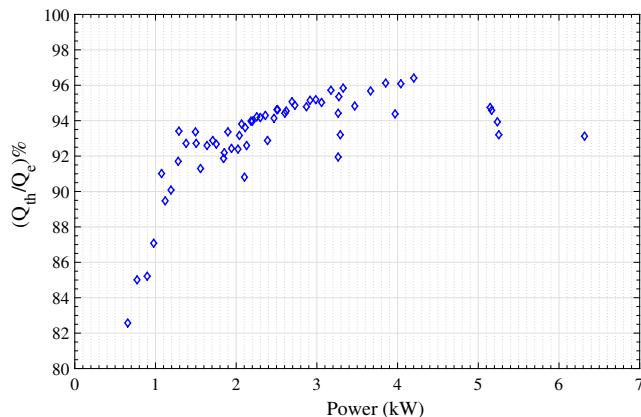


Fig. 7. The difference between the imposed electric power and the deposited thermal power.

temperature, aluminum block temperature, pressure, and mass flow rate), and derived parameters (heat flux, mass flux, and wall temperature). The uncertainties of the derived parameters were analyzed according to the procedure proposed by Moffat [38]:

$$\delta R = \left(\sum_{i=1}^n \left(\frac{\partial R}{\partial X_i} \delta X_i \right)^2 \right)^{\frac{1}{2}} \quad (21)$$

where δR is the uncertainty result of the dependent variable, R is the result of a calculation based on one or more measurements, X_i is the i th independent variable, δX_i is the uncertainty of i th variable, and n is the number of the independent variables. The uncertainty of the heat flux, mass flux, wall temperature were estimated as $\pm 0.52\%$, $\pm 2.13\%$, and $\pm 4.2\%$. Table 4 summarizes the uncertainty results.

2.6. Experiment procedure

Before conducting the experiments, a degassing process was performed to eliminate the effect of non-condensable gases on the wall superheat that is required for bubble nucleation. The working fluid was circulated through the facility and heated up to around 80°C ; then, it was allowed to boil on the heated surface for approximately 45 min, which led to a release of the dissolved gases and any entrapped air on the surface of the heater. After the degassing process, the inlet conditions were first maintained at a specific subcooled temperature and mass flow rate, by adjusting the preheater and the pump circulation speed, respectively. At the same time, the imposed heat flux was adjusted by varying the

Table 4
Uncertainty analysis results for experimental parameters.

Parameter	Uncertainty
<i>Geometry parameter</i>	
Channel width	$\pm 0.05\text{ mm}$
Channel thickness	$\pm 0.05\text{ mm}$
Heated length	$\pm 0.05\text{ mm}$
Heated width	$\pm 0.05\text{ mm}$
<i>Measured parameter</i>	
Inlet and outlet temperature	$\pm 1.1^\circ\text{C}$ [$\pm 0.4\%$]
Aluminum block temperature	$\pm 0.5^\circ\text{C}$ [$\pm 0.2\%$]
Pressure	$\pm 0.1\%$
Flow rate	$\pm 0.08\%$
<i>Derived parameter</i>	
Heat flux	$\pm 0.52\%$
Mass flux	$\pm 2.13\%$
Wall temperature	$\pm 4.2\%$

electrical current and voltage from the DC power supply. During the initial stages, the flow through the channel must be in the single-phase liquid region.

In the present study, the experiment was performed under two different conditions. In the first case, the flow rate was fixed and the heat flux was increased slowly at a constant rate (approximately 0.4 kW/min). During the experiment, the data were saved directly using the DAQ system. In the second case, the heat flux was kept constant and the mass flux was decreased in a stepwise manner, starting from a high mass flow rate that ensured the flow was single-phase. At each step, and once the reading from all TCs had stabilized over 2–3 min, the temperature, mass flow rate, pressure, and power data were stored using the DAQ system.

3. Results and discussion

The ONB, OSV, and OFI were experimentally investigated through a vertical narrow rectangular channel. The following subsections achieve the following: (a) discuss the experimental results for the constant mass flow rate and constant heat flux procedures, as well the consistency between these methods; (b) provide comparisons with existing correlations and other experimental data; and (c) propose a new empirical correlation.

3.1. Constant mass flow rate

The experimental results obtained at a constant mass flow rate while increasing the heat flux are illustrated in Fig. 8. The ONB incipience was identified using the wall temperature deviation method as the intersection of the single-phase and two-phase heat transfers. The slope of the wall temperature deviated simultaneously with the occurrence of bubbles on the heated surface, as shown in picture (1) in Fig. 8. As the heat flux increased, the bubble diameter, bubble site density, and bubble generation rate increased, which led to a continuous enhancement of the heat transfer rate. As a result, the wall temperature almost remained constant between point (1) and point (2) in Fig. 8. As the heat flux increased, the bubble departure diameter increased as well. Once the bubble diameter became larger than the thermal boundary layer thickness, the condensation rate increased, owing to the high degree of subcooling. Therefore, the bubble existence rate on the heated surface remained constant and/or slightly increased with the heat flux between point (2) and point (3); in this region, the heat transfer rate remained constant and/or slightly increased. As a result, the slope of the wall temperature increased. The starting point (2) where the slope deviates (slightly increases) is considered to be the OSV. Besides, the pressure drop slightly decreased with the heat flux until the ONB. After bubble generation, the pressure drop slightly increased and almost remained constant after the OSV. As the heat flux was increased further, the bubbles were dramatically generated, and the void fraction increased. At the point (3), the inlet pressure fluctuated as the pressure drop rapidly increased with an increase in the heat flux. Thus, the flow across the coolant channel became unstable. Moreover, the slope of the wall temperature slightly decreased owing to heat transfer enhancement. This point (3) at which inlet pressure deviation rapidly increased at the same time as the pressure drop was identified as the OFI. The high subcooled inlet temperature ($35\text{--}65^\circ\text{C}$) explains the very low values of the void fraction, i.e., the void fraction did not grow significantly because of the high subcooled temperature.

For low mass fluxes, the OSV and OFI occurred at approximately the same point. On the other hand, the heat flux that was required to transfer downstream flows from ONB to OFI reduced once the inlet temperature increased, as illustrated in Fig. 9. For instance,

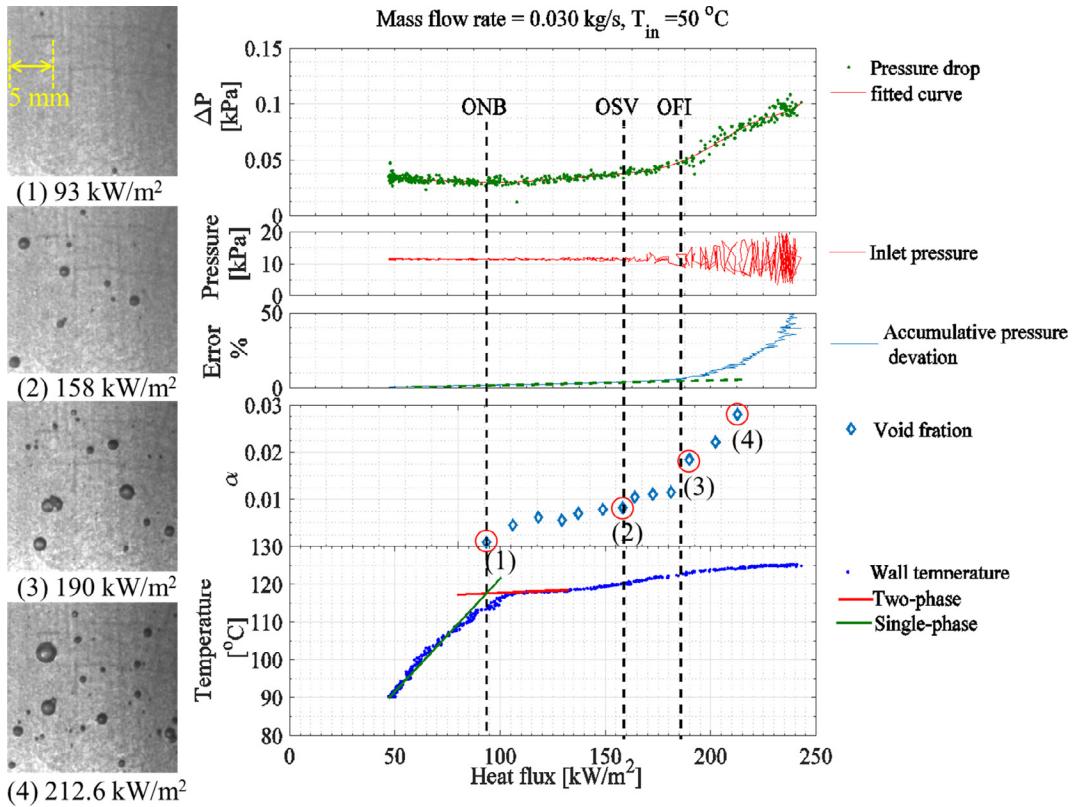


Fig. 8. Evolution of thermal hydraulic parameters from single-phase flow to flow instability under constant mass flow rate pressure.

after the ONB, approximately 99 kW/m^2 should be added to the surface to reach the OFI for inlet temperature equal to 35°C . However, the OFI occurred after the ONB after 65 kW/m^2 were added when the inlet temperature was 65°C . Interestingly, the difference between the ONB heat flux and the OFI heat flux increased once the mass flow rate increased, as shown in Fig. 10. For example, 96 kW/m^2 should be added to move from the ONB to the OFI at 0.03 kg/s , while approximately 190 kW/m^2 should be added if the mass flow rate is 0.10 kg/s . The figure shows that, for high mass flow rates, the OSV occurred much earlier than the OFI. However, if the inlet temperature was greater than 50°C , the results showed that the OSV and OFI occurred at the same point.

Fig. 11 shows the wall temperatures when the ONB and the OFI occur. However, the OSV data were limited by the experimental operation conditions, for that they merged with the OFI data for all mass flow rates with an inlet temperature higher than 50°C , and for all inlet temperatures with mass flow rates lower than 0.06 kg/s . The wall temperature at the ONB and the OFI increased with the heat flux. Furthermore, the ONB wall temperature was more dependent on the inlet temperature than on the OFI. The influence of mass flow rate and inlet temperature on the ONB and the OFI heat fluxes is shown in Fig. 12. The ONB and the OFI heat fluxes reduced once the inlet temperature increased and/or the mass flow rate decreased. At a fixed mass flow rate, the superheat wall temperature that was required to initiate boiling on the heated surface was approximately constant, because the liquid film temperature at the heated surface was equal to the saturation temperature. Accordingly, the imposed heat that was used to raise the liquid film temperature from the subcooled status to the saturated status reduced when the inlet temperature increased. The ONB and the OFI heat fluxes increased when the mass flow rate increased. As the increase in the mass flow rate enhanced the heat transfer, more heat was required to achieve a high superheat wall temperature to

initiate the ONB and the OFI. Moreover, the higher mass flow rate led to a higher wall temperature at the ONB and the OFI, as shown in Fig. 13. The parametric trends of inlet temperature and mass flow rate for OFI and ONB were similar.

3.2. Constant heat flux

The experimental data obtained with a constant heat flux and a decreasing mass flow rate are shown in Fig. 14. For single-phase flow, the system was stable and the pressure drop was directly proportional to the mass flow rate. As the mass flow rate was reduced, bubbles were generated on the heated surface. At that point, the pressure drop slightly increased; thus, the slope of the pressure drop curve reduced. The point where the pressure drop curve deviated from the single-phase line was identified as the incipience of the ONB. Additionally, the wall temperature increased once the mass flow reduced owing to reduction in the heat transfer coefficient. After the bubbles were generated, the increase in the wall temperature reduced owing to the existence of bubbles on the heated surface. Further reduction in the mass flow rate led to an increase in the bubble departure diameter and the bubble generation rate, and owing to the highly subcooled bulk temperature, the bubbles condensed directly, a process during which the heat transfer coefficient almost remained constant and/or slightly increased. Thus, the negative slope of the wall temperature increased again. The OSV was considered to be the second deviation of the wall temperature slope, as a significant generation of bubbles reflects the behavior of the heat transfer process. At this point, the slope of the pressure drop curve reduced once again; however, it remained positive. As the mass flow rate was reduced further, the bubbles grew dramatically, and the slope kept reducing until it reached a zero value. Afterward, the slope of the pressure drop curve became negative, because the pressure drop

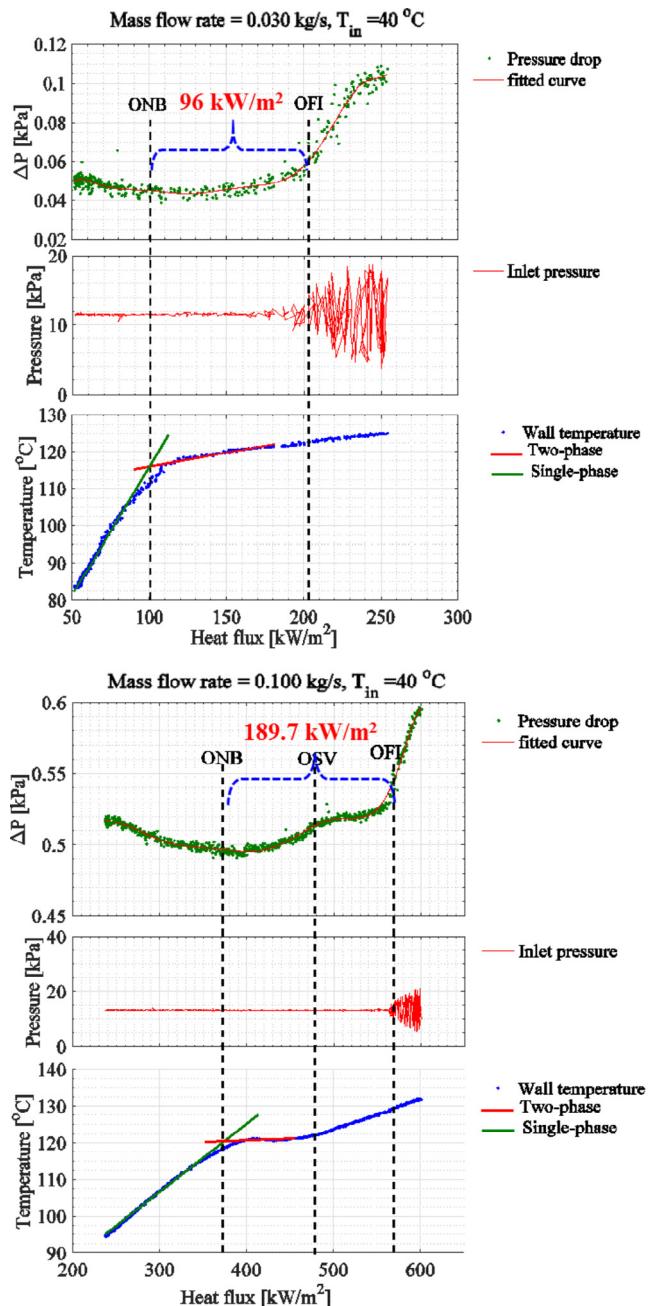
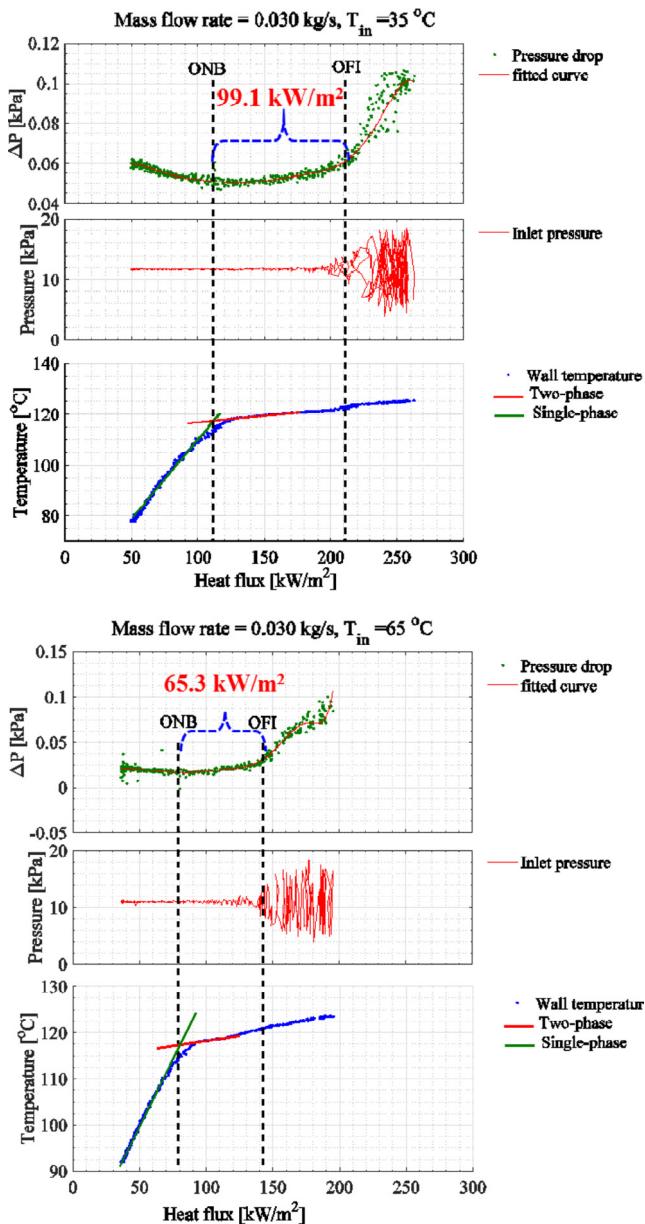


Fig. 9. The influence of inlet temperature on the heat flux required to proceed from the OFI to the ONB.

increased as the mass flux reduced. The minimum point in the pressure drop-mass flow rate curve where the slope is equal to zero was considered to be the OFI.

The goal of this experimental procedure was to identify the OFI, even though both the ONB and OSV were observed. For high heat fluxes, the two-phase flow was established at a higher mass flow rate; thus, the OFI occurred at a higher mass flow rate as the imposed heat flux increased, as shown in Fig. 15. Moreover, the pressure drop at the OFI decreased with the heat flux, as the OFI mass flow rate had decreased. The figure shows that the relation between the mass flow rate and the pressure drop is approximately independent of the imposed heat flux in the single-phase region. With more reduction in the heat flux, the OFI occurred at a much lower mass flow rate. The pressure drop reduced to nearly zero without its slope becoming negative, i.e., the pressure drop did not increase again after the OFI, as shown in Fig. 16. For very low heat fluxes, the OFI was identified as the point where the inlet pressure started to fluctuate. The figure shows that the OFI

Fig. 10. The influence of mass flow rate on the heat flux required to proceed from the OFI to the ONB.

occurred at a slightly higher mass flow rate when the inlet temperature increased, i.e., once the inlet temperature increased, the OFI occurred earlier. At a constant heat flux, the increment in the bulk temperature was constant. Accordingly, at higher inlet temperatures, the wall superheat temperature and the local bulk temperature were higher; therefore, the OFI occurred earlier.

3.3. Consistency between constant mass flow rate and constant heat flux approaches

The consistency between the two experimental methods is shown in Fig. 17. When a 319 kW/m^2 constant heat flux was applied to the heated surface with an inlet temperature of 50°C , the OFI occurred at a mass flow rate of 0.06 kg/s , as shown in Fig. 17(a). When the same inlet temperature of 50°C was used with a mass flow rate of 0.06 kg/s , the OFI was achieved at a heat flux of

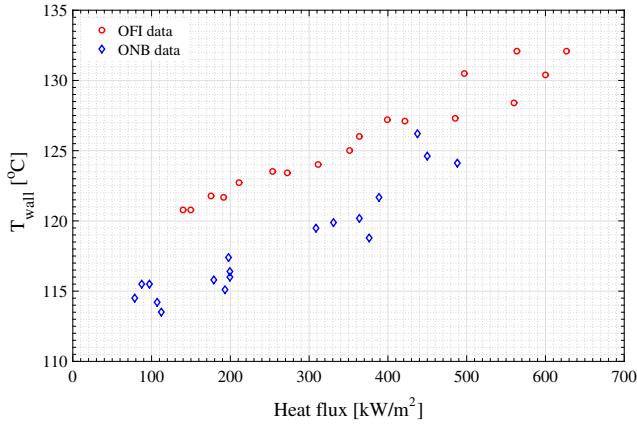


Fig. 11. The effect of heat flux on the wall temperature at the ONB and OFI.

318 kW/m², as shown in Fig. 17(b). The consistency of the ONB and OSV were checked by introducing a specific energy ratio:

$$e = \frac{q''A_h}{\dot{m}} \quad (22)$$

The specific energy at the ONB for the constant heat flux procedure is 3295 kJ/kg, which was almost similar to the specific energy at the ONB for the constant mass flow rate procedure (3306 kJ/kg). Likewise, the specific energy at the OSV was equal to approximately 4530 kJ/kg for the constant heat flux case, and approximately 4580 kJ/kg for constant mass flow rate case. Thus, the ONB, OSV, and OFI can be experimentally achieved either by keeping the mass flow rate constant and increasing the heat flux, or keeping the heat flux constant and decreasing the mass flow rate.

3.4. Comparison with relevant experiments and correlations

The experimental data of ONB incipience were compared with the ONB correlations that were proposed by Bergles and Rohsenow

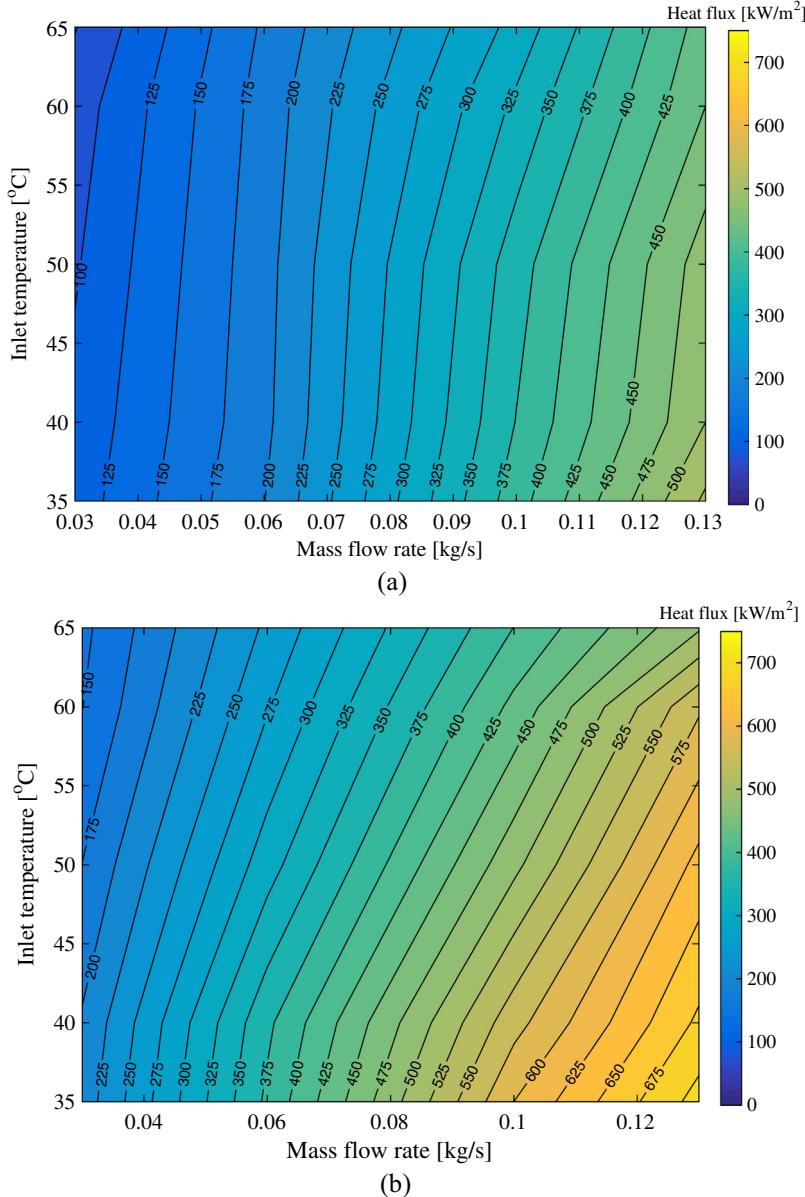


Fig. 12. The influence of inlet temperature and mass flow rate on (a) ONB heat flux, and (b) OFI heat flux.

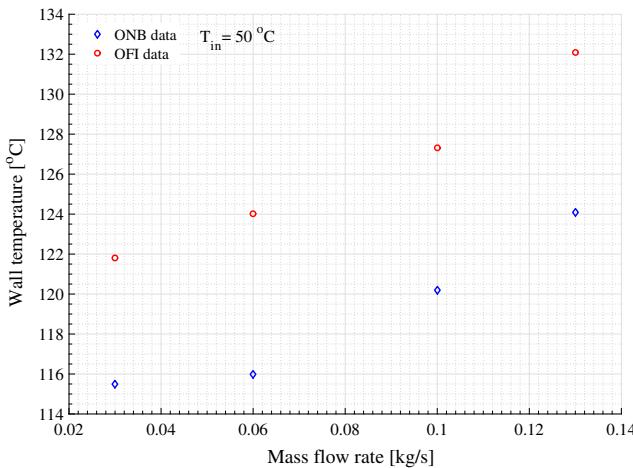


Fig. 13. The effect of mass flow rate on the wall temperature at the ONB and OFI.

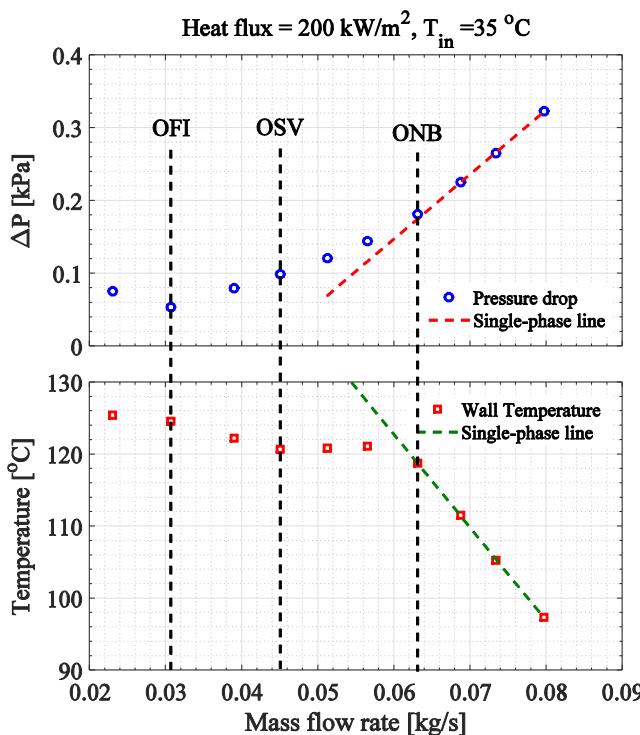


Fig. 14. Evolution of thermal hydraulic parameters from single-phase flow until flow instability under constant heat flux.

[9], Jens and Lottes [10], Thom et al. [11], and Yang et al. [22], as depicted in Fig. 18. Jens and Lottes's [10] correlation predicted the experimental data within an error of $\pm 20\%$. However, other correlations tended to underestimate the experimental data. The underprediction may have occurred because of different geometries and operation conditions. In addition, other results of other experimental studies were compared against the present experimental data, as shown in Fig. 19. The current experimental results were in good agreement with the results of Sudo et al. [12] and Song et al. [39], in which they followed Jens and Lottes' [10] correlation. However, owing to the differences in the experiment parameters, the results of Wang et al. [21] show that the ONB occurs at a lower wall superheat temperature.

Fig. 20(a) shows comparisons between the OFI experimental results for the constant heat flux approach and the correlations

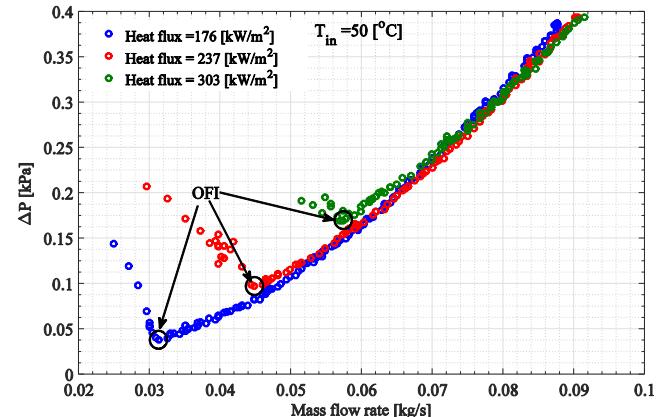


Fig. 15. The influence of the heat flux on the pressure drop-mass flow rate curve.

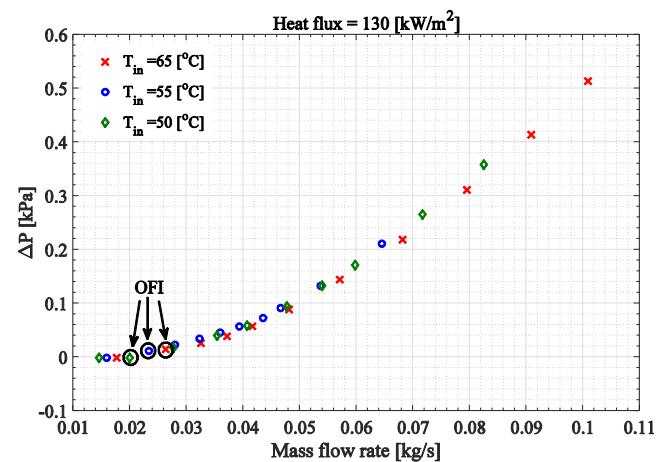


Fig. 16. The influence of inlet temperature on the pressure drop-mass flow rate curve under low heat flux.

proposed by Whittle and Forgan [6], Kennedy et al. [37], Lee et al. [1], Unal [33], the modified Bowring model [36], and the modified Saha and Zuber model [36]. The last three OSV models were utilized to predict the OFI data. As the experimental results demonstrated that OSV and OFI may occur at the same point owing to the very high subcooled temperature, in which equilibrium equality at the channel exit is a mostly negative value, the OSV at the channel exit was assumed to be related to the OFI. Mass flux G_{OFI} was, therefore, derived as

$$G_{OFI} = \frac{q''A_h}{A_s C p_l [(T_{sat} - \Delta T_{sub(OSV)}) - T_i]} \quad (23)$$

The Lee et al. [1] correlation and the modified Bowring and modified Saha and Zuber models [36] predicted the present experimental data within an error of $\pm 20\%$. However, the significant deviation between the experimental data and the predictions of the other correlations may have been due to different heating conditions. Following the same modification procedure that was proposed by Wang et al. [36], the correlations that were proposed by Whittle and Forgan [6], Kennedy et al. [37], and Unal [33] were modified to consider the effect of a surface heated on one-side, as follows;

$$R = \frac{T_{out} - T_{in}}{T_{sat} - T_{in}} = \frac{1}{1 + 25D_h L_h} \left(\frac{P_w}{P_h} \right) \quad (24)$$

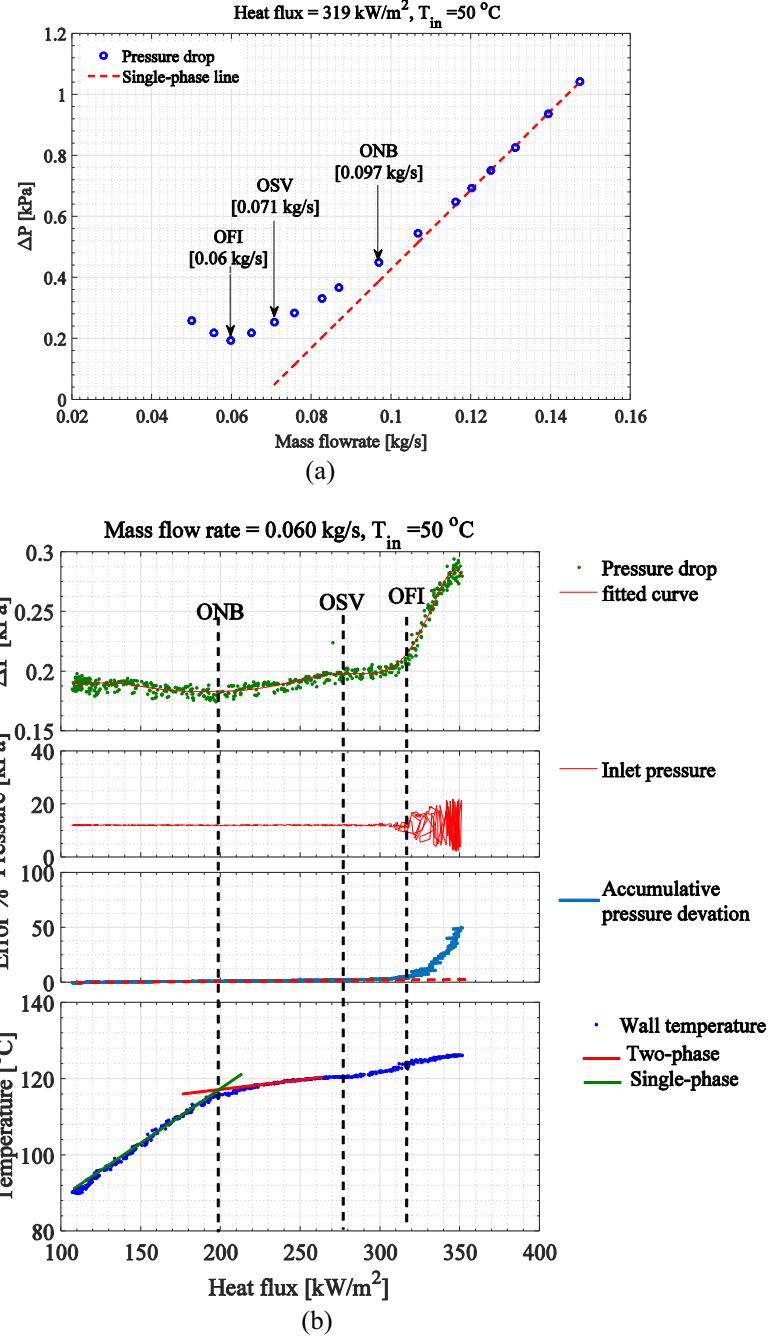


Fig. 17. Consistency between (a) the constant heat flux approach and (b) the constant mass flux approach.

$$G_{OFI} = 1.11 G_{sat} \left(\frac{P_w}{P_h} \right) \quad (25)$$

rate approach, the previous modified OSV models and the OFI correlations could estimate the OFI heat flux, as shown in Fig. 21. Thereby, Eq. (23) was rearranged to evaluate q''_{OFI} as follows

$$\begin{aligned} \Delta T_{sub(OSV)} &= 0.24 \frac{q''}{h} \left(\frac{P_w}{P_h} \right) \quad V \geq 0.45 \text{ m/s} \\ \Delta T_{sub(OSV)} &= 0.11 \frac{q''}{h} \left(\frac{P_w}{P_h} \right) \quad V < 0.45 \text{ m/s} \end{aligned} \quad (26)$$

As shown in Fig. 20(b), a reasonable agreement exists between the present data and the modified correlations for predicting the OFI, within an error of $\pm 20\%$. Similarly, for the constant mass flow

$$q''_{OFI} = \frac{GA_s C p_l [(T_{sat} - \Delta T_{sub(OSV)}) - T_i]}{A_h} \quad (27)$$

The comparison showed good agreement with the present experimental data for low heat fluxes. However, as the imposed heat flux increased, the modified correlation of Whittle and Forgan slightly overpredicted the experimental data. When the same cor-

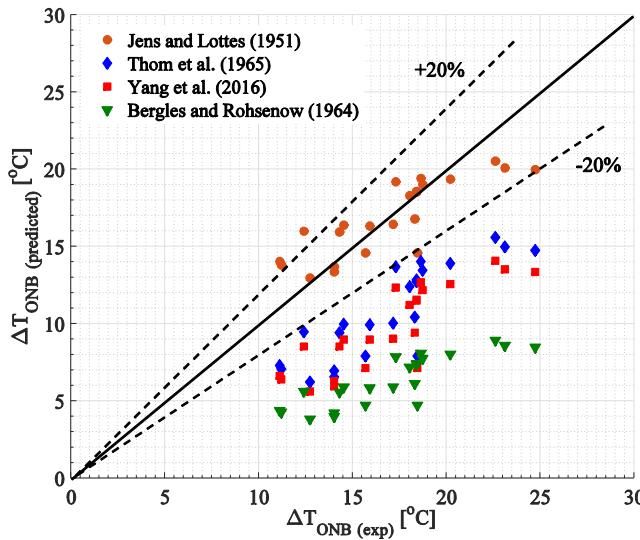


Fig. 18. Comparison between the experimental and the predicted ONB data.

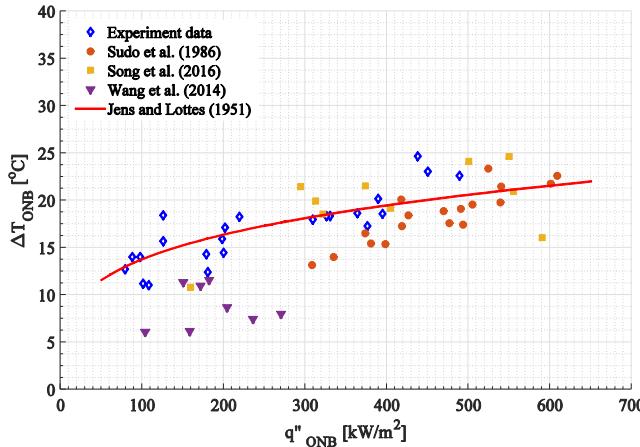


Fig. 19. Comparison between the present experimental data and data from other researchers' experiments.

relations were used to predict the OFI data under constant heat flux conditions and/or constant mass flow rate condition, a consistency between the two experiment procedures was revealed.

3.5. New empirical correlations

The data analysis with the related correlations implies that the OFI conditions are highly dependent on the saturation conditions. For instance, G_{OFI} and q''_{OFI} are the predicted terms of G_{sat} and q''_{sat} , respectively. This relationship between flow instability and saturation conditions can be utilized to develop a correlation for estimating the heat flux at the OFI within a narrow rectangular channel that is heated from one-side. Beside the saturation parameter, the bubble behavior depends significantly on the system pressure [40]. Once the system pressure increases, the bubble diameter and the bubble life time decrease. In which high heat flux is required to achieve the OFI (close to the heat flux at the saturation condition, q''_{sat}). When the system pressure decreases, the bubble diameter and bubble life time increases. Thus, the OFI occurs at conditions much far from the saturation condition. Therefore, the new OFI correlation considers the pressure in the flow channel as a dependent parameter as follows:

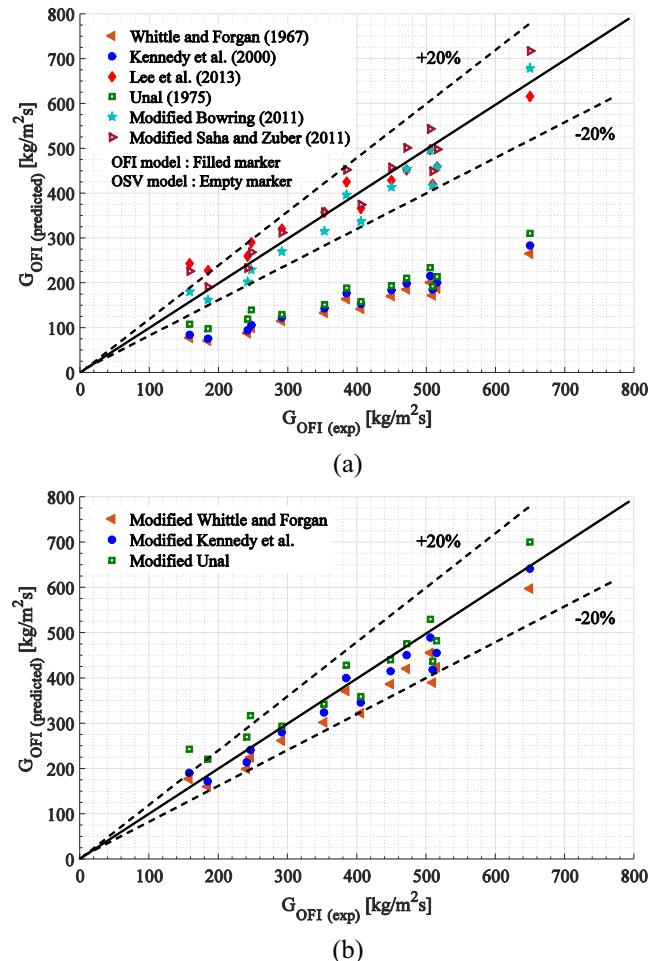


Fig. 20. Comparison between the experimental and the predicted OFI data under constant heat flux: (a) unmodified correlations and (b) modified correlations.

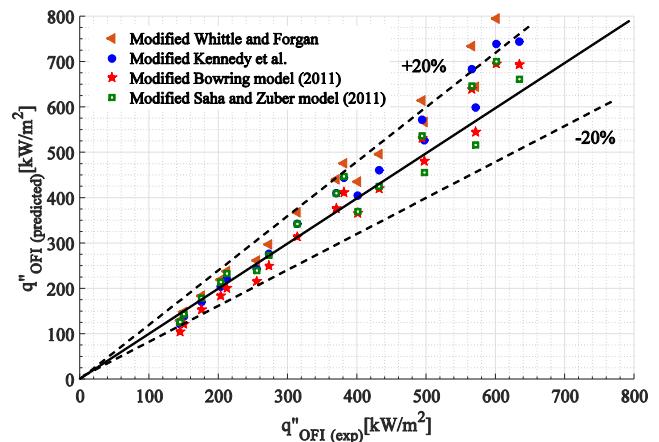


Fig. 21. Comparison between the experimental data and the modified correlations under constant mass flow rate.

$$\frac{q''_{OFI}}{q''_{sat}} = 0.8 \left(\frac{P_h}{P_w} \right) \left(\frac{P}{1.12} \right)^{0.4} \quad (28)$$

where P is the pressure in bar, and q'' is the heat flux in kW/m^2 . The new correlation predicts the present experimental data (~ 1 bar exit pressure) and Wang et al. [36] experimental data (~ 10 bars exit pressure) within an error of $\pm 12\%$, as illustrated in Fig. 22. The

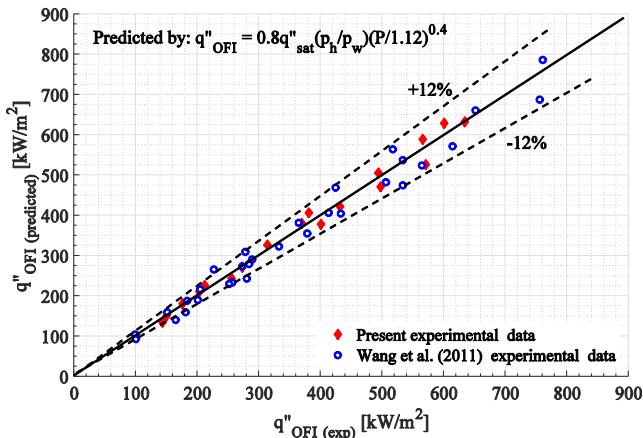


Fig. 22. New proposed OFI correlation with experimental data under constant mass flow rate.

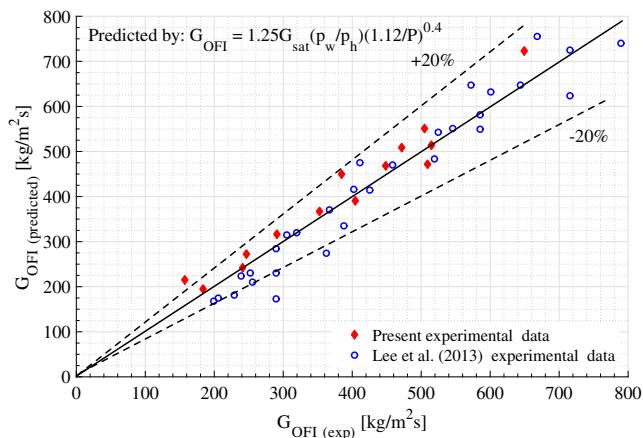


Fig. 23. New proposed OFI correlation with experimental data under constant heat flux.

new proposed correlation is applicable to narrow rectangular channels that are heated on one-side or two-sides, if the ratio between heated and wetted perimeter ($\frac{P_h}{P_w}$) is taken. Alternatively, for the constant heat flux approach, Eq. (28) can be rewritten as

$$\frac{G_{OFI}}{G_{sat}} = 1.25 \left(\frac{P_w}{P_h} \right) \left(\frac{1.12}{P} \right)^{0.4} \quad (29)$$

The correlation reasonably predicts the present OFI experimental data and Lee et al. [1] experimental data under constant heat flux conditions within an error of $\pm 20\%$, as shown in Fig. 23.

4. Conclusions

In the present study, subcooled flow boiling thermal hydraulic phenomena, i.e., the ONB, OSV, and OFI, in a narrow rectangular channel heated from one-side were experimentally investigated. The experiment was performed for upward flow under atmospheric pressure. Two different experimental procedures were conducted to approach and identify the ONB, OSV, and OFI: the constant mass flow rate approach and constant heat flux approach. The slope of the wall temperature was used to determine the ONB and OSV. On the other hand, the slope of the pressure drop curve and inlet pressure fluctuation were used to determine the OFI. The conclusions of this research study are summarized as follows:

- (1) The existence of bubbles on the heated surface enhanced the heat transfer coefficient. Thus, the slope of the wall temperature reduced. On the other hand, the pressure drop slightly increased after the ONB.
- (2) The OSV preceded the OFI for high mass flow rates and/or low inlet temperatures. However, they merged to the same point at low mass flow rates and/or high inlet temperatures, at which the bubbles on the heated surface dramatically increased, causing significant growth in the void fraction and flow instability. However, at high subcooled temperatures, the void fraction did not increase significantly.
- (3) The margin range between the ONB and OFI reduced once the inlet temperature increased and/or the mass flow rate increased. The increase in the mass flow rate led to an increase in the ONB and OFI heat fluxes, wall temperature at the ONB and OFI, and the pressure drop at the OFI. However, the inlet temperature had the opposite effect.
- (4) For the constant heat flux experimental procedure, the slope of the pressure drop curve can be used to identify the ONB. The mass flow rate and the pressure drop at the OFI increased with the heat flux, and a similar trend was observed with the inlet temperature. On the other hand, the pressure drop at the OFI reached zero without increasing again after the OFI for low imposed heat fluxes.
- (5) The results show consistency between the two different experimental procedures. Similar correlations were used to predict the data of both procedures, and they proved the consistency. Some correlations were modified to fit the effect of a surface heated on one-side. After the modification, the experimental data were predicted within an error of $\pm 20\%$. A new empirical correlation was proposed to predict the OFI heat flux and OFI mass flux with better accuracy. The proposed correlation is applicable for high subcooled temperature upward flow through narrow rectangular channel that is heated either from one-side or two-sides. The new correlation was compared with the present data and experimental data done by other researchers, and the comparison showed good agreement within an error of $\pm 12\%$.

Acknowledgement

This research was supported by Basic Science Research Program through the National Research Foundation of Korea (NRF) funded by the Ministry of Science, ICT & Future Planning (NRF-2015R1C1A1A02037095).

Conflict of interest

The authors declared that there is no conflict of interest.

References

- [1] J. Lee, H. Chae, S.H. Chang, Flow instability during subcooled boiling for a downward flow at low pressure in a vertical narrow rectangular channel, *Int. J. Heat Mass Transfer* 67 (2013) 1170–1180.
- [2] A. Ghione, B. Noel, P. Vinai, C. Demaziere, Criteria of onset of flow instability in heated vertical narrow rectangular channels at low pressure: an assessment study, *Int. J. Heat Mass Transfer* 100 (2017) 464–478.
- [3] Y.Y. Hsu, On the size of active nucleation cavities on a heating surface, *ASME J. Heat Transfer* 84 (1962) 207–216.
- [4] G. Yadigaroglu, Two-phase flow instabilities and propagation phenomena, in: M. Delhaye, M. Giot, L.M. Riethmuller (Eds.), *Thermohydraulics of Two-Phase Systems for Individual Design and Nuclear Engineering*, Hemisphere, Washington, DC, 1981, pp. 353–403.
- [5] J.A. Boure, A.E. Bergles, L.S. Tong, Review of two-phase flow instability, *Nucl. Eng. Des.* 25 (1973) 165–192.
- [6] R.H. Whittle, R. Forgan, A correlation for the minima in the pressure drop versus flow-rate curves for sub-cooled water flowing in narrow heated channels, *Nucl. Eng. Des.* 6 (1967) 89–99.

- [7] L.C. Ruspini, C.P. Marcel, A. Clausse, Two-phase flow instabilities: a review, *Int. J. Heat Mass Transfer* 71 (2014) 521–548.
- [8] E.J. Davis, G.H. Anderson, The incipience of nucleate boiling in forced convection flow, *AIChE J. Heat Transfer* 12 (1966) 774–780.
- [9] A.E. Bergles, W.M. Rohsenow, The determination of forced-convection surface-boiling heat transfer, *ASME J. Heat Transfer* 86 (1964) 365–372.
- [10] W.H. Jens, P.A. Lottes, Argonne National Laboratory Report, ANL-4627, 1951, Argonne National Laboratory.
- [11] J.R.S. Thom, W.M. Walker, T.A. Fallon, G.F.S. Reising, Boiling in subcooled water during flow up heated tubes or annuli, in: Symposium on Boiling Heat Transfer in Steam Generating Units and Heat Exchangers, Manchester, 15–16 September 1965, IMechE, London.
- [12] Y. Sudo, K. Miyata, H. Ikawa, M. Kaminaga, Experimental study of incipient nucleate boiling in narrow vertical rectangular channel simulating subchannel of upgraded JRR-3, *J. Nucl. Sci. Technol.* 23 (1986) 73–82.
- [13] W. Tong, A.E. Bergles, M.K. Jensen, Pressure drop with highly subcooled flow boiling in small-diameter tubes, *Exp. Therm. Fluid. Sci.* 15 (1997) 202–212.
- [14] S.M. Ghiaasiaan, R.C. Chedester, Boiling incipience in microchannels, *Int. J. Heat Mass Transfer* 45 (2002) 4599–4606.
- [15] I. Hapke, H. Boye, J. Schmidt, Onset of nucleate boiling in minichannels, *Int. J. Therm. Sci.* 39 (2000) 505–513.
- [16] S.Y. Su, S.Y. Huang, X.M. Wang, Study of boiling incipience and heat transfer enhancement in forced flow through narrow channels, *Int. J. Multiphase Flow* 31 (2005) 253–260.
- [17] R. Ahmadi, A. Nouri-Borujerdi, J. Jafari, I. Tabatabaei, Experimental study of onset of subcooled annular flow boiling, *Progr. Nucl. Energy* 51 (2009) 361–365.
- [18] O.S. Al-Yahia, D. Jo, Onset of Nucleate Boiling for subcooled flow through a one-side heated narrow rectangular channel, *Ann. Nucl. Energy* 109 (2017) 30–40.
- [19] C.P. Yin, Y.Y. Yan, T.F. Lin, B.C. Yang, Subcooled flow boiling heat transfer of R-134a and bubble characteristics in a horizontal annular duct, *Int. J. Heat Mass Transfer* 43 (2001) 1885–1896.
- [20] Y.Y. Hsieh, L.J. Chiang, T.F. Lin, Subcooled flow boiling heat transfer of R-134a and the associated bubble characteristics in a vertical plate heat exchanger, *Int. J. Heat Mass Transfer* 45 (2002) 1791–1806.
- [21] C. Wang, H. Wang, S. Wang, P. Gao, Experimental study of boiling incipience in vertical narrow rectangular channel, *Ann. Nucl. Energy* 66 (2014) 152–160.
- [22] L.X. Yang, A. Guo, D. Liu, Experimental investigation of subcooled vertical upward flow boiling in a narrow rectangular channel, *Exp. Heat Transfer* 29 (2016) 221–243.
- [23] O. Zeitoun, M. Shoukri, On the net vapour generation phenomenon in subcooled flow boiling, in: Proceedings of the Engineering Foundation Conference on Convective Flow Boiling, Alberta, Canada, 1995.
- [24] G.F. Hewitt, P.B. Whalley, Advanced optical instrumentation methods, *Int. J. Multiphase Flow* 6 (1980) 139–156.
- [25] J.M. Delhayé, Optical methods in two-phase flow, in: Proc. Dynamic Flow Conf., Dynamic Measurements unsteady Flow, 1978, pp. 321–343.
- [26] G.F. Hewitt, D.N. Roberts, Studies of Two-Phase Flow Patterns by Simulations X-Ray and Flash Photography, Report AERE-M2159, UKAEA, Harwell.
- [27] A.V. Smith, Fast response multi-beam X-ray absorption technique for identifying phase distribution during steam-water blowdowns, *J. Br. Nucl. Energy Soc.* 14 (1975) 227–235.
- [28] C. Piper, Final report on the semi-scale gamma attenuation two-phase water density measurement, Microfiche No IN-1487, 1974.
- [29] M. Lamari, Design, Construction and Commissioning of a Two-Phase (air-water) Flow Regime Transition Test Rig, Master Thesis, Carleton University, Ottawa, Dept. of Mech. & Aero. Engineering, 1991.
- [30] R.W. Bowring, Physical model based on bubble detachment and calculation of steam voidage in subcooled region of a heated channel, Institute for Atomenergi, Halden, Norway, Report No. HPR-10, 1962.
- [31] P. Saha, N. Zuber, Point of net vapor generation and vapor void fraction in subcooled boiling, in: Proceedings of the 5th International Heat Transfer Conference, Tokyo, Japan, vol. 4, 1974, pp. 175–179.
- [32] S. Lee, S. Bankoff, A comparison of predictive models for the onset of significant void at low pressures in forced-convection subcooled boiling, *J. Mech. Sci. Technol.* 12 (1998) 504–513.
- [33] H.C. Unal, Determination of the initial point of net vapor generation in flow boiling systems, *Int. J. Heat Mass Transfer* 18 (1975) 1095–1099.
- [34] Z. Edelman, E. Elias, Void fraction distribution in low flow rate subcooled boiling, *Nucl. Eng. Des.* 66 (1981) 375–392.
- [35] M. Kureta, T. Hibiki, K. Mishima, H. Akimoto, Study on point of net vapor generation by neutron radiography in subcooled boiling flow along narrow rectangular channels with shot heated length, *Int. J. Heat Mass Transfer* 46 (2003) 1171–1181.
- [36] J. Wang, Y. Huang, Y. Wang, Visualized study on specific points on demand curves and flow patterns in a single-side heated narrow rectangular channel, *Int. J. Heat Fluid Flow* 32 (2011) 982–992.
- [37] J.E. Kennedy, G.M. Roach Jr., M.F. Dowling, S.I. Abdel-Khalik, S.M. Ghiaasiaan, S. M. Jeter, et al., The onset of flow instability in uniformly heated horizontal microchannels, *ASME J. Heat Transfer* 122 (2000) 118–125.
- [38] R.J. Moffat, Describing the uncertainties in experimental results, *Exp. Therm. Fluid Sci.* 1 (1988) 3–17.
- [39] J.H. Song, J. Lee, Y.H. Jeong, S.H. Chang, Onset of nucleate boiling for downward flow in narrow rectangular channels under low Pressure, International topical meeting on nuclear reactor thermal hydraulics, operation and safety NUTHOS-11, Gyeongju, Korea, October 9–13, 2016.
- [40] Y. Cao, Z. Kawara, T. Yokomine, T. Kunugi, Visualization study on bubble dynamical behavior in subcooled flow boiling under various subcooling degree and flowrates, *Int. J. Heat Mass Transfer* 93 (2016) 839–852.